Journal of Electroceramics, 13, 613–618, 2004

Oxygen Permeation Properties of Ceria-Ferrite-Based Composites

H. TAKAMURA,[1,2] K. OKUMURA,[1] Y. KOSHINO,[1] A. KAMEGAWA[1,2] & M. OKADA[1,2]
[1]*Department of Materials Science, Graduate School of Engineering, Tohoku University, Aoba-yama 02, Aoba-ku, Sendai 980-8579, Japan*
[2]*CREST, JST, Japan*

Submitted February 13, 2003; Revised March 13, 2004; Accepted March 19, 2004

Abstract. The oxygen flux density of $Ce_{0.8}Gd_{0.2}O_{1.9}$–x vol% $MnFe_2O_4$ (CGO-xMFO) composite-type ceramics membranes has been investigated. The samples and reforming catalysts were prepared by the Pechini process. For the CGO-xMFO composites, oxygen permeation was observed even at $x = 3$ vol%, presumably due to the presence of grain boundary phases. For CGO-15MFO, the n-type electronic conductivity was found to be dominant at 900°C or higher. The thickness dependence of jO_2 revealed that surface exchange kinetics was significantly involved in the case of the membrane thickness of $L < 0.5$ mm. The highest oxygen flux density of 10 μmol·cm^{-2}·s^{-1} was achieved for CGO-15MFO with the 10 mass% Ni-Pr:CeO_2 catalyst ($L = 0.25$ mm) at 1000°C and a flow rate of 270 sccm.

Keywords: oxygen permeable membranes, composites, doped ceria, spinel-type ferrite, partial oxidation of methane

Introduction

Oxygen separation membranes based on mixed oxygen-ion and electronic conductors are of interest, in view of their promising applications, such as production of pure oxygen from air and syngas from methane [1]. Perovskite-type oxides in La-Sr-Co-Fe and La-Sr-Ga-Fe systems are well known to exhibit a high oxygen flux density, jO_2, at elevated temperatures [2, 3]. For example, $La_{0.7}Sr_{0.3}Ga_{0.6}Fe_{0.4}O_{3-\delta}$ exhibits a high oxygen flux density of approximately 8.2 μmol·cm^{-2}·s^{-1} at 1000°C under methane conversion atmosphere [3]. In addition to those, dual-phase-type mixed conductors comprising of ionic and electronic conductive phases have been developed. For example, composites consisting of Gd-doped CeO_2 (CGO) as an ion-conductive matrix and Sr-doped $LaMnO_3$ (LSM) or Ca-doped $GdCoO_3$ (GCC) responsible for electronic conduction have been reported to exhibit a superior mixed conductivity and the resulting high oxygen flux density [4, 5]. As a novel member of composite-type mixed conductors, recently, CGO-15 vol% $MnFe_2O_4$ (MFO) was found to show a high jO_2 of 7 μmol·cm^{-2}·s^{-1} at 1000°C under methane conversion tests [6]. However, the nature of this composite including the effect of volume fraction of MFO on jO_2, electrical conductivity and rate-determining process, remains unknown.

Thus, the purpose of this study is to firstly evaluate the oxygen flux density of CGO-MFO composites in the context of volume fraction of the electronic conductive MFO phase, and then to consider their electrical conductivity and rate-determining process based on the membrane thickness dependence of jO_2. Moreover, the enhancement of jO_2 under methane conversion atmosphere was examined in view of reforming catalyst supports.

Experimental Details

The composites of $Ce_{0.8}Gd_{0.2}O_{1.9}$–x vol% $MnFe_2O_4$ ($1 \leq x \leq 50$) were prepared by the Pechini process [6–9]. Raw materials used were nitrates and hydroxides serving as metal sources, and citric acid and ethylene glycol serving as chelating agents. After polymerizing, carbonizing, and calcination at 700°C, oxide powders were finally sintered at 1300°C for 2 h. Reforming catalysts were also prepared by the same technique. The catalysts evaluated were 10 mass% Ni supported on either CeO_2 or $(Ce_{0.8}RE_{0.2})O_{2-\delta}$ where RE = Pr, Sm

or Gd. In the case of catalyst preparation, carbonized powders were calcined at 1000°C. The resultant catalyst powders were tape-cast on composite disks to be around 200 μm in thickness.

Electrical conductivity was measured by means of the four-probe DC technique at 800–1000°C. For the electrical measurement, partial oxygen pressure, pO_2, was varied in the range of 0.21–10^{-12} atm. The setup for oxygen permeation and methane conversion tests was described elsewhere [10]. Diamond-polished (both sides) samples of approximately ϕ 8 mm × 0.1–1 mm in thickness were sealed with gold and borosilicate glass rings. The samples were then subjected to various pO_2 gradients between air and either He, Ar-5%H_2, or Ar-10%CH_4 within the temperature range of 800–1000°C. Sweep gases were fed at a rate of 20–270 sccm. Gas concentration was determined by use of a gas chromatograph and a mass spectrometer. For methane conversion tests, Ar-5%H_2 gas was swept to activate the catalyst prior to Ar-10%CH_4 gas flow. In this case, oxygen flux densities were calculated from concentrations of CO and CO_2, and CO selectivity was calculated as follows:

$$\text{CO selectivity}\,(\%) = [\text{CO}]/([\text{CO}] + [\text{CO}_2]) \times 100 \quad (1)$$

where [CO] and [CO_2] denote concentrations of the respective gases.

Results and Discussion

First of all, phase identification was performed for CGO–x vol% MFO (CGO-xMFO), where $1 \leq x \leq 50$. From XRD analyses, the composites with $x = 5$ or higher were found to comprise of CGO and MFO phases. In addition, a small amount of $GdFeO_3$ was observed. As well as CGO–$CoFe_2O_4$ (CFO) composites in the previous work [6], the lattice constant of fluorite-type CGO phase was found to decrease, compared to that of pure CGO. The formation of $GdFeO_3$, which would reduce the Gd content in CGO, may be responsible for decrease in the lattice constant.

The oxygen flux density of CGO-MFO was evaluated as a function of volume fraction of MFO as shown in Fig. 1. The oxygen permeation property was measured within the temperature range of 800–1000°C under Ar-10%CH_4 (20 sccm) / air gradients. The oxygen flux density was multiplied by a thickness of L for comparison. As expected, for 1 vol% MFO

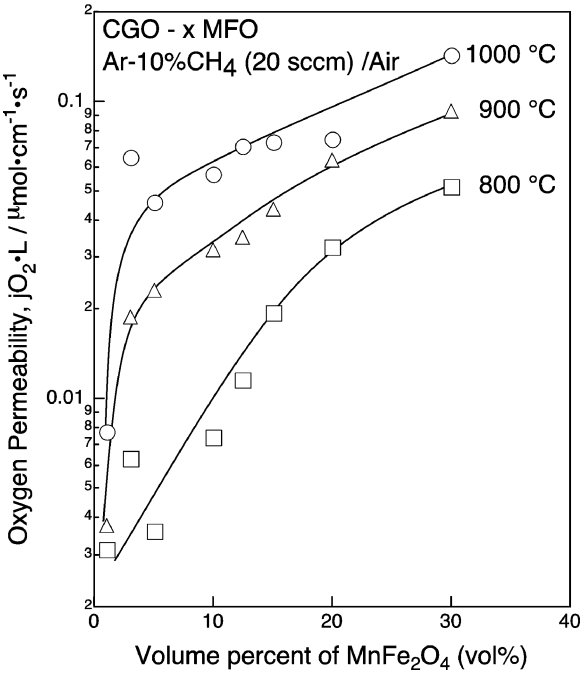

Fig. 1. The oxygen permeability, $jO_2 \times L$, of CGO-xMFO as a function of the volume fraction of MFO. $T = 800$, 900, and 1000°C.

sample, the permeability is limited to less than 1×10^{-8} mol·cm^{-1}·s^{-1} due to the lack of electronic conductivity; however, CGO-MFO was found to be oxygen permeable even at 3 vol% MFO. This volume fraction is considerably lower than that of percolation threshold, which is expected to be around 25 vol%. This behavior will be discussed in the context of the formation of grain boundary phase later. The $jO_2 \times L$ value increases with increasing the volume fraction of MFO up to 30 vol%. However, CGO-MFO membranes with 40 vol% MFO or higher caused fracture during the methane conversion test. Figure 2 shows the TEM micrograph of CGO-17CFO fired at 1300°C. Even though CGO usually requires a high sintering temperature such as 1600°C for densification, ceria-spinel-ferrite-based composites are found to be well densified by firing at 1300°C for 2 h. This decrease in the sintering temperature is presumably due to the presence of spinel-type ferrite that can work as a sintering agent. As a result of low-temperature sintering, a fine grain size of less than 500 nm was obtained. In addition, somewhat different contrasts were observed around grain boundary regions. By taking dark-field images, the grain boundary phase was found to consist of nano-sized CGO and spinel-type ferrite grains, but not $GdFeO_3$. This grain

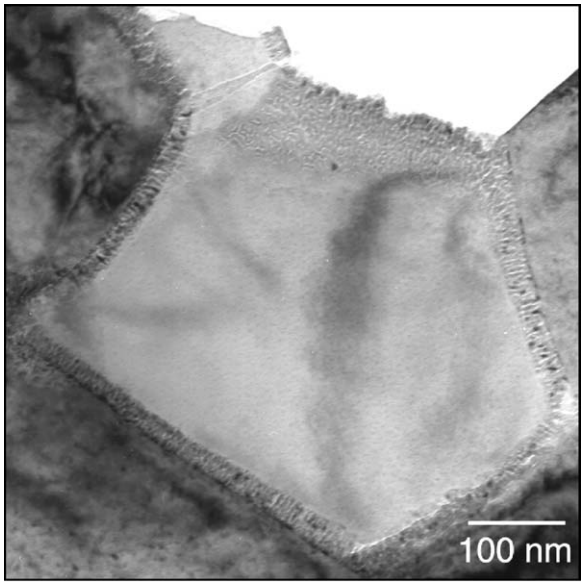

Fig. 2. TEM micrograph of CGO-17MFO fired at 1300°C for 2 h.

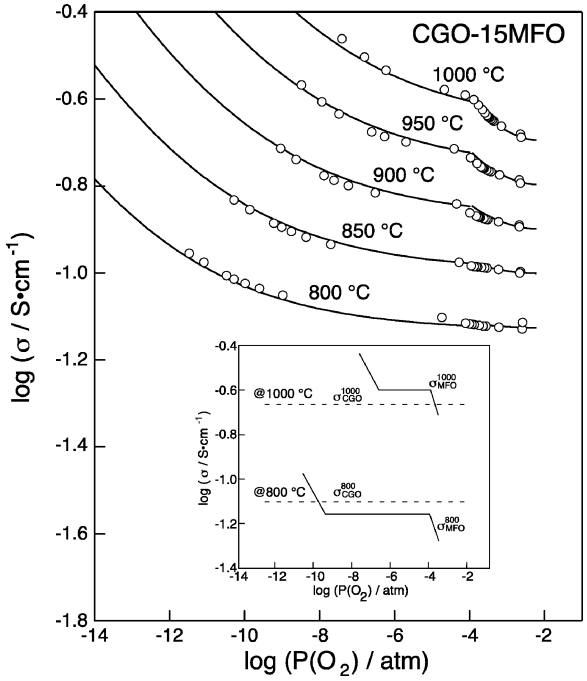

Fig. 3. The conductivity isotherms of CGO-15MFO taken at temperatures ranging from 800 to 1000°C. The inset shows a schematic illustration of conductivity isotherms at 800 and 1000°C for explanation.

boundary phase seems to be responsible for oxygen permeation at a lower volume fraction of electronic conductive phase.

The total electrical conductivity of CGO-MFO was evaluated as a function of temperature and pO_2. Figure 3 shows conductivity isotherms of CGO-15MFO at temperatures ranging from 800 to 1000°C. The reversibility of σ as a function of pO_2 was confirmed by returning to a reference point at $pO_2 \approx 10^{-3}$ atm. A plateau regime followed by upturned increase in total σ with decreasing pO_2 was observed at 800°C, while additional increase in σ emerged at $pO_2 \approx 10^{-4}$ atm at 900°C or above. Given that spinel-type ferrites tend to show n-type behavior [6], changes in the shape of conductivity isotherms can be explained as follows: n-type conductivity originating from MFO is slightly lower than ionic conductivity of CGO at 800°C except for a low pO_2 region; as temperature increases, the n-type conductivity of MFO starts to become a major carrier at a wide pO_2 region as a result of difference in activation energies, i.e. $\Delta E_n^{\mathrm{MFO}} > \Delta E_i^{\mathrm{CGO}}$. This scenario is schematically illustrated in Fig. 3. If this is the case, upturned increase in σ at low pO_2 is attributed to the reduction of MFO. It should be also noted that n-type conduction is dominant at temperatures above 900°C, and as a result, the oxygen permeation of CGO-MFO should be limited by its effective ionic conductivity, i.e. volume fraction $\times\, \sigma_i^{\mathrm{CGO}}$ when the rate-determining process is the bulk diffusion. The effective ionic conductivity and rate-determining process were then considered in view of the membrane thickness dependence of jO_2.

Figure 4 shows the oxygen flux density of CGO–15MFO as a function of membrane thickness, L, at temperatures ranging from 800 to 1000°C. The sweep gas used was Ar-5%H_2 in order to simplify the calculation of pO_2 of the permeate side. The oxygen flux density (left axis) increases with decreasing L; for example, the jO_2 values were 2.0 and 2.7 μmol·cm^{-2}·s^{-1} for $L = 1.0$ and 0.67 mm, respectively. However, as expected, jO_2 as a function of L tends to be flatten as the membrane thickness decreases to less than 0.5 mm, presumably due to the involvement of surface exchange kinetics. Solid lines for jO_2 were obtained by fitting the following equation proposed by Bouwmeester et al. at given temperatures [11]:

$$jO_2 = -\gamma \frac{RT}{4^2 F^2 L} \int_{\ln pO_2'}^{\ln pO_2''} \frac{\sigma_e \sigma_i}{\sigma_e + \sigma_i} d \ln pO_2 \qquad (2)$$

where σ_i and σ_{el} denote ionic conductivity and

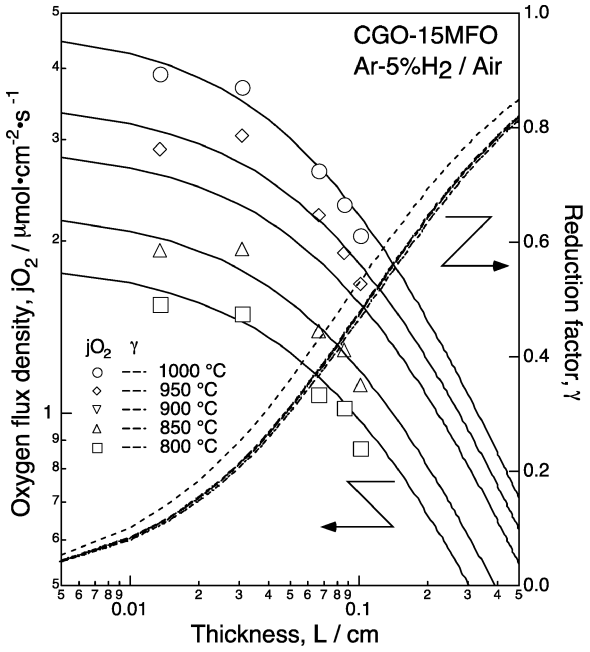

Fig. 4. The oxygen flux density and reduction factor of CGO-15MFO as a function of the membrane thickness. $T = 800$–1000°C.

electronic conductivity, pO_2' and pO_2'' denote partial oxygen pressures at the feed and permeate sides, and T, L, R, F denote temperature, membrane thickness, the gas constant, and the faraday constant, respectively. In addition, a factor of γ can be express as follows:

$$\gamma = \frac{1}{1 + (2L_c/L)} \tag{3}$$

where L_c means a characteristic thickness. The factor of γ can be regarded as a sort of "reduction factor" that restricts the oxygen flux density due to surface exchange kinetics. Assuming that the ambipolar conductivity term is approximated by the ionic conductivity that is independent on pO_2, one can obtain:

$$jO_2 \approx -\gamma \frac{RT}{4^2F^2L}\sigma_i \ln\left(\frac{pO_2''}{pO_2'}\right) \tag{4}$$

In the fitting procedures, L_c, and a theoretical oxygen permeability term were used as adjusting parameters. As a fitting result, L_c was estimated to be around 0.5 mm regardless of temperature. The reduction factor of γgas also plotted in Fig. 4 as dotted lines (right axis). For example, the value of γ was found to be 0.53 for $L = 1.0$ mm at 1000°C. This implies that jO_2 observed at 1000°C and $L = 1.0$ mm is only 53% of the theoretical jO_2 value. Moreover, σ_i in Eq. (4) can be calculated by using the theoretical oxygen flux density, pO_2' and pO_2''. The value of pO_2'' was estimated from gas concentration of H_2 and H_2O. For example, σ_i estimated from the theoretical oxygen flux density was 0.18 S/cm at 1000°C, showing a good agreement with the expected effective ionic conductivity of $0.85 \times 0.24 = 0.20$ S/cm. However, to further discuss about L_c, another experimental results, for example, by means of conductivity relaxation techniques will be needed. In any case, apart from the L_c value obtained by the fitting procedure, jO_2 was obviously saturated at around $L < 0.5$ mm in Fig. 4. This implies that, as well as other MIEC-based oxygen permeable ceramics, the rate-determining process of CGO-MFO shifts from bulk diffusion to surface exchange kinetics as the membrane thickness decreases.

The effect of catalyst supports on the oxygen flux density of CGO-MFO under methane conversion atmosphere was also considered. Among a number of reforming catalyst supports, CeO_2 is well known as a promoter which gives high CO selectivity. The possible mechanism for giving high CO selectivity is proposed in the context of oxygen nonstoichiometry of CeO_2 as follows [12]:

$$CeO_2 + nCH_4 \rightarrow CeO_{2-n} + nCO + 2nH_2 \tag{5}$$

$$CeO_{2-n} + nCO_2 \rightarrow CeO_2 + nCO \tag{6}$$

RE-substituted CeO_2 supports, where RE = Pr, Sm, and Gd, were prepared in this study, and the oxygen flux density of CGO-15MFO with those reforming catalysts was evaluated. The amount of Ni-catalyst was fixed to 10 mass%. Figures 5(a) and (b) show the jO_2 of CGO-15MFO with the 10Ni-RE:CeO_2 catalysts ($L = 0.25 \pm 0.01$ mm) as a function of temperature and the corresponding CO selectivity, respectively. Compared to CeO_2 without RE dopants, doped-CeO_2, especially Pr:CeO_2, shows a high oxygen flux density and CO selectivity at elevated temperatures. Unlike Sm:CeO_2 and Gd:CeO_2, Pr:CeO_2 is known to be an n-type electronic conductor even at high pO_2 region [13]. This unique behavior may be relevant to the high jO_2 and CO selectivity. For the CGO-15MFO with the 10Ni-RE:CeO_2 catalysts, the flow rate dependence of jO_2 and CO selectivity at 1000°C was plotted in Figs. 6 (a) and (b), respectively. The highest jO_2 of 10 μmol·cm^{-2}·s^{-1} was attained at 1000°C and a

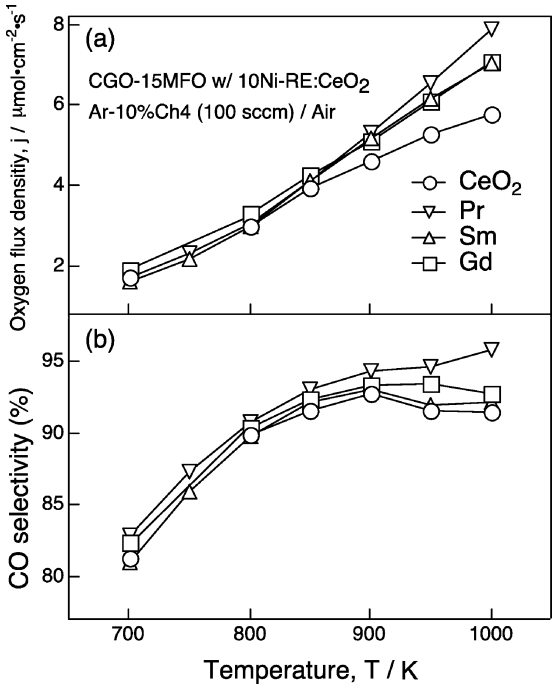

Fig. 5. The temperature dependence of (a) the oxygen flux density and (b) CO selectivity of CGO-15MFO with 10Ni-RE:CeO_2 catalysts ($L = 0.25 \pm 0.01$ mm), where RE = Pr, Sm or Gd.

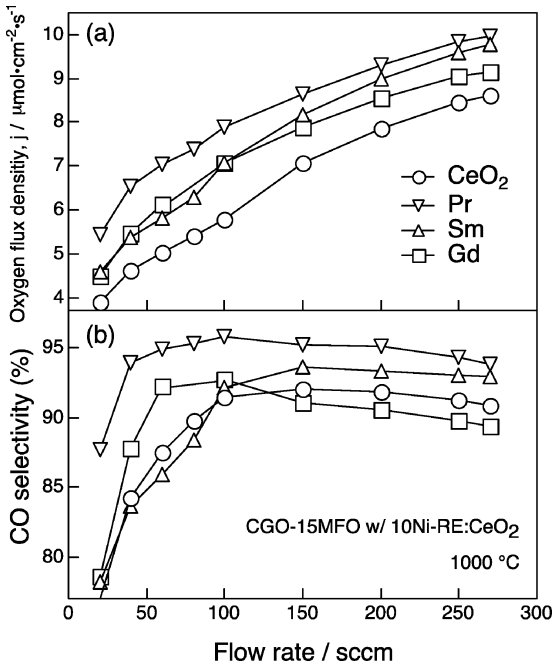

Fig. 6. The flow rate dependence of (a) the oxygen flux density and (b) CO selectivity of CGO-15MFO with 10Ni-RE:CeO_2 catalysts ($L = 0.25 \pm 0.01$ mm), where RE = Pr, Sm or Gd. $T = 1000$°C.

flow rate of 270 sccm for CGO-15MFO with the 10Ni-Pr:CeO_2 catalyst. Even though a relatively high temperature of 1000°C and a thinner membrane thickness of ≈ 0.25 mm are required, this oxygen flux density is comparable to those for the perovskite-type oxides such as $La_{0.7}Sr_{0.3}Ga_{0.6}Fe_{0.4}O_{3-\delta}$ (8.2 μmol·cm^{-2}·s^{-1} at 1000°C [3]) and $Ba_{0.5}Sr_{0.5}Co_{0.8}Fe_{0.2}O_{3-\delta}$(8.6 μmol·cm^{-2}·s^{-1} at 875°C [14]).

Conclusions

The oxygen flux density, jO_2, of $Ce_{0.8}Gd_{0.2}O_{1.9}$–x vol% $MnFe_2O_4$ (CGO-xMFO) was examined in the context of volume fraction of MFO, membrane thickness of L, and reforming catalysts. For the CGO-xMFO composites, oxygen permeation phenomena was observed even at $x = 3$ vol%, presumably due to the presence of grain boundary phases. For CFO-15MFO, the n-type electronic conductivity was found to be dominant at 900°C or higher. The thickness dependence of jO_2 revealed that surface exchange kinetics was significantly involved in the case of $L < 0.5$ mm. The highest jO_2 of 10 μmol·cm^{-2}·s^{-1} was attained at 1000°C and a flow rate of 270 sccm for CGO-15MFO with the 10Ni-Pr:CeO_2 catalyst.

Acknowledgments

This work has been supported by CREST of Japan Science and Technology Corporation (JST) and Ministry of Education, Science, Sports and Culture, Grant-in-Aid for Young Scientists (B), No. 15760512.

References

1. P.N. Dyer, R.E. Richards, S.L. Russek, and D.M. Taylor, *Solid State Ionics*, **134**, 21 (2000).
2. Y. Teraoka, H.M. Zhang, S. Furukawa, and N. Yamazoe, *Chem. Lett.*, 1743 (1985).
3. T. Ishihara, Y. Tsuruta, T. Todaka, H. Nishiguchi, and Y. Takita, *Solid State Ionics*, **152/153**, 709 (2002).
4. V.V. Kharton, A.V. Kovalevsky, A.V. Viskup, F.M. Figueiredo, A.A. Yaremchenko, E.N. Naumovich, and F.M.B. Marques, *J. Eur. Ceram. Soc.*, **21**, 1763 (2001).
5. U. Nigge, H.-D. Wiemhöfer, E.W.J. Römer, H.J.M Bouwmeester, and T.R. Schulte, *Solid State Ionics*, **146**, 163 (2002).
6. H. Takamura, M. Kawai, K. Okumura, A. Kamegawa, and M. Okada, in *Solid State Ionics — 2002*: *Mat. Res. Soc. Symp. Proc.*,

edited by P. Knauth, J.-M. Tarascon, E. Traversa, and H.L. Tuller (Materials Research Society, Warrendale, 2003), vol. 756, p. EE8.11.1.
7. M.P. Pechini and U.S. Patent #3,330,697 (1967).
8. H. Takamura and H. L. Tuller, *Solid State Ionics*, **134**, 67 (2000).
9. H. Takamura, K. Enomoto, A. Kamegawa, and M. Okada, *Solid State Ionics*, **154**, 581(2002).
10. H. Takamura, K. Enomoto, Y. Aizumi, A. Kamegawa, and M. Okada, *Solid State Ionics*, in press.
11. H.J.M. Bouwmeester, H. Kruidhof, and A.J. Burggraaf, *Solid State Ionics*, **72**, 185 (1994).
12. K. Otsuka, T. Ushiyama, and I. Yamanaka, *Chem. Lett.*, 1517 (1993).
13. T.S. Stefanik and H.L. Tuller, in *Solid State Ionics — 2002*: *Mat. Res. Soc. Symp. Proc.*, edited by P. Knauth, J.-M. Tarascon, E. Traversa, and H.L. Tuller (Materials Research Society, Warrendale, 2003), vol. 756, p. EE10.8.1.
14. Z.P. Shao, G.X. Xiong, H. Dong, W.H. Yang, and L.W. Lin, *Separation and Purification Technology*, **25**, 97 (2001).